HHS Public Access

Author manuscript

Brain Behav Immun. Author manuscript; available in PMC 2024 August 01.

Published in final edited form as:

Brain Behav Immun. 2023 August ; 112: 220–234. doi:10.1016/j.bbi.2023.06.011.

Fibroblast-derived PI16 sustains inflammatory pain via regulation of CD206^{+} myeloid cells

Rachelle Garrity[a,1], **Neha Arora**[a,1], **Md. Areeful Haque**[a], **Drew Weis**[a], **Ronnie T. Trinh**[a], **Sanjay V. Neerukonda**[b], **Susmita Kumari**[a], **Ibdanelo Cortez**[a], **Eroboghene E. Ubogu**[c], **Rajasekaran Mahalingam**[a], **Diana Tavares-Ferreira**[b], **Theodore J. Price**[b], **Annemieke Kavelaars**[a], **Cobi J. Heijnen**[a,d], **Andrew J. Shepherd**[a,2]

[a.] Laboratories of Neuroimmunology, Department of Symptom Research, Division of Internal Medicine, University of Texas MD Anderson Cancer Center, Houston, TX.

[b.] Department of Neuroscience and Center for Advanced Pain Studies, University of Texas at Dallas, Richardson, TX.

[c.] Neuromuscular Immunopathology Research Laboratory, Division of Neuromuscular Disease, Department of Neurology, University of Alabama at Birmingham, Birmingham, AL.

[d.] Department of Psychological Sciences, Rice University, Houston, TX.

Abstract

Originally identified in fibroblasts, Protease Inhibitor (PI)16 was recently shown to be crucial for the development of neuropathic pain via effects on blood-nerve barrier permeability and leukocyte infiltration, though its impact on inflammatory pain has not been established. Using the complete Freund's Adjuvant inflammatory pain model, we show that *Pi16*$^{-/-}$ mice are protected against sustained inflammatory pain. Accordingly, intrathecal delivery of a PI16 neutralizing antibody in wild-type mice prevented sustained CFA pain. In contrast to neuropathic pain models, we did not observe any changes in blood-nerve barrier permeability due to PI16 deletion. Instead, *Pi16*$^{-/-}$ mice display reduced macrophage density in the CFA-injected hindpaw. Furthermore, there was a significant bias toward CD206^{hi} (anti-inflammatory) macrophages in the hindpaw and associated dorsal root ganglia. Following CFA, intrathecal depletion of CD206^{+} macrophages using mannosylated clodronate liposomes promoted sustained pain in *Pi16*$^{-/-}$ mice. Similarly, an IL-10 neutralizing antibody also promoted sustained CFA pain in the *Pi16*$^{-/}$ when administered intrathecally. Collectively, our results point to fibroblast-derived PI16 mediating substantial differences in macrophage phenotype in the pain neuroaxis under conditions of inflammation.

[2.] To whom correspondence should be addressed: Andrew J. Shepherd, Laboratories of Neuroimmunology, Department of Symptom Research, the University of Texas MD Anderson Cancer Center, Unit 1055, 6565 MD Anderson Boulevard, Houston, Texas 77030. Telephone: +1 (713) 745-7959 Fax: +1 (832) 750-5153 ajshepherd@mdanderson.org.

[1]These authors contributed equally to this study.

Declaration of Competing Interest

The authors declare that they have no known competing financial interests or personal relationships that could have appeared to influence the work reported in this paper.

The co-expression of PI16 alongside fibroblast and macrophage markers in human DRG raise the likelihood that a similar mechanism operates in human inflammatory pain states. Collectively, our findings may have implications for targeting fibroblast-immune cell crosstalk for the treatment of chronic pain.

Keywords

PI16; Complete Freund's Adjuvant; pain; inflammation; fibroblast; macrophage; blood-nerve barrier; meninges; CD206; IL-10

1. Introduction

In the United States, more than 50 million people live with chronic pain, and more than 19 million people have high impact chronic pain requiring ongoing treatment (Dahlhamer, Lucas et al. 2018, Yong, Mullins et al. 2022). The sub-optimal efficacy and side-effect profiles of current analgesics (e.g. nonsteroidal anti-inflammatory drugs, gabapentinoids, SNRIs and opioids) necessitates discovery of novel pain targets and ultimately therapeutic candidates with fewer side effects.

In our previous investigation, we identified a novel regulator of pain named protease/peptidase inhibitor 16 (PI16). PI16 was originally identified as a contributor to pain in DRG samples from *Grk2*$^{+/-}$ mice that develop persistent pain in response to transient inflammation. In our prior study, PI16-deficient mice were protected against spared nerve injury (SNI)-induced neuropathic pain (Singhmar, Trinh et al. 2020). Our observations support a model where nerve injury augmented PI16 production by meningeal and epi/perineurial fibroblasts, thereby enhancing endothelial barrier permeability and facilitating immune cell infiltration into the DRG and nerve, enhancing neuropathic pain. PI16 is also called CD364, CRISP9, PSPBP, or MSMBBP and is a member of the cysteine-rich secretory proteins, antigen 5, and pathogenesis-related 1 proteins (CAP) superfamily and has homologues in other mammalian species including rats and humans. It is mostly expressed by cardiac fibroblasts, which secrete PI16 to the interstitium through a glycophosphatidylinositol (-GPI) membrane anchor (Regn, Laggerbauer et al. 2016). Although comprehensive understanding of the biological roles of PI16 is still lacking, it has been identified as a prognostic marker in recurrent prostate cancer, correlating positively with relapse-free survival (Reeves, Xuan et al. 2005, Reeves, Dulude et al. 2006). PI16 was also identified in cardiomyocytes as a secreted, growth-inhibiting factor (Frost and Engelhardt 2007, Deng, Yang et al. 2020). In addition, PI16 identified a regulatory T-cell subset with reduced forkhead box P3 expression which is theorized to facilitate autoimmunity in type 1 diabetes (Hope, Welch et al. 2019). In our prior study, PI16-deficient mice were protected against spared nerve injury (SNI)-induced neuropathic pain (Singhmar, Trinh et al. 2020). Given the fundamental differences in the etiologies of inflammatory and neuropathic pain (Xu and Yaksh 2011), we used the complete Freund's adjuvant (CFA)-induced pain model in this study to elucidate the role of PI16 in chronic inflammatory pain. We demonstrate that PI16-deficient mice are protected against sustained inflammatory pain

and that deletion of PI16 from fibroblasts upregulates CD206^{hi} macrophage accumulation in the mouse skin and DRG to enhance recovery from CFA-induced inflammatory pain.

2. Materials and methods

2.1. Animals:

Male and female 8–12-week-old C57BL/6J mice homozygous for the global deletion of *Pi16* (Modified Medical Research Council [MMRC] stock no. 032520-UCD) were used as experimental mice. C57BL/6J mice, 8–12 weeks of age, obtained from Jackson Laboratories were used as wild-type controls. *Pi16*-floxed [*Pi16*$^{fl/fl}$; MGI:6114785, (Regn, Laggerbauer et al. 2016)] were bred to B6.129-*Gt(ROSA)26Sor*$^{tm1(cre/ERT2)Tyj}$/J mice (stock no. 008463) to produce an inducible *Pi16* conditional knock-out strain. These same *Pi16*$^{fl/fl}$ mice were also bred to *Col1a2*-cre/ERT,-ALPP)7Cpd/J mice (stock no. 029235; (Zheng, Zhang et al. 2002)) to produce a tamoxifen-inducible, fibroblast-specific *Pi16* conditional knockout strain. Inducible global and fibroblast specific knockouts were compared to their Cre-ER-negative littermates as controls.

Experiments in this study were performed in accordance with the National Institute of Health *Guidelines for the Care and Use of Laboratory Animals* and the Ethical Issues of the International Association for the Study of Pain and were approved by the local Institutional Animal Care and Use Committee. Animals were housed in a 12/12 h day/night cycle, with free access to food and water. Animals were randomly assigned into groups and experimenters were blinded to genotype groups. Complete blinding to intraplantar injection (CFA versus vehicle) is not attainable in the acute phase post-injection, due to overt differences in hindpaw erythema and edema. To induce Cre recombination, tamoxifen (Sigma-Aldrich, T5648) was dissolved in corn oil (Sigma-Aldrich, C8267) at 5 mg/mL by mixing overnight at 37°C in a light-protected vessel. Mice received an intraperitoneal (i.p.) 50 mg/kg dose for 5 consecutive days. Control mice received an equivalent dose of corn oil vehicle.

2.2. Inflammatory Pain Model

Mice were anesthetized with 2–3% isoflurane in oxygen delivered through a nose cone. No analgesics were administered after intraplantar injections. 5 μl of Complete Freund's Adjuvant (Sigma-Aldrich F5881) was injected into the mid-plantar surface of both hindpaws with a Hamilton microsyringe fitted with a 27-gauge needle. Control groups received a 5 μL intraplantar injection of sterile 1x PBS into the mid-plantar surface of both hindpaws. Mannosylated clodronate liposomes were performed using the mannosylated macrophage depletion kit (CLD-8914, Encapsula Nano Sciences) as described previously (Niehaus, Taylor-Blake et al. 2021). Mice received 3 intrathecal injections (5 μl each) using a Hamilton microsyringe. Intrathecal goat anti-IL-10 IgG was also delivered via three 5 μl (10μg) intrathecal injections as described previously (Krukowski, Eijkelkamp et al. 2016).

2.3. Assessment of Pain-Related Behaviors

2.3.1. Measurement of Mechanical Hypersensitivity—Paw withdrawal threshold (PWT) was assessed at baseline and over time using calibrated Semmes-Weinstein von

Frey filaments. The mechanical force required to provoke a paw withdrawal response was determined using the “up-down” method (Chaplan, Bach et al. 1994). Data are depicted as the group mean by averaging the threshold obtained for left and right hindpaws for each mouse. Male and female cohorts of mice were tested separately on the same days between 07:30 and 09:30h.

2.3.2. Measurement of Thermal Hypersensitivity—Paw withdrawal latency (PWL) to radiant heat was measured at baseline and over time using the Hargreaves’ device (IITC Life Science Inc., Woodland Hills, CA, USA). Mice were placed on a pre-warmed glass plate (29–31°C) in transparent enclosures (Hargreaves, Dubner et al. 1988). After a 30-minute habituation period, a halogen light beam (Set to an intensity 20% of maximum) was applied to the plantar surface of both hindpaws. A 20-second cutoff time was used to avoid potential overheating and tissue damage. Three trials at intervals of 10–15 minutes were performed on each hindpaw and averaged together to estimate the mean PWL to thermal stimulus for each mouse. Data represents the group mean by averaging the latency across both left and right hindpaws for each mouse.

2.3.3. Paw Edema—To measure paw edema, mice were manually restrained and a digimatic micrometer (Bel-Art Scienceware 134160001) was used to measure paw thickness in millimeters at baseline and over time. Measurements were taken 24, 48, and 72 h post-intraplantar injection. Data represents the group mean by averaging the threshold across both left and right hindpaws for each mouse.

2.4. Western blotting

A Biorupter (Diagenode) was used to prepare lysates of sciatic nerve and DRG in RIPA buffer (10 mM Tris-HCl, pH 6.8, 100 mM NaCl, 1 mM EDTA, 10% glycerol, 1% Triton X-100, 0.1% SDS, 0.5% sodium deoxycholate, 2 mM Na3VO4, 50 mM NaF) supplemented with protease and phosphatase inhibitors. Protein content was analyzed using a Bicinchoninic acid assay as previously described (Singhmar, Trinh et al. 2020). Lysates matched for total protein content were run on sodium dodecyl sulfate-polyacrylamide gels, transferred to polyvinylidene difluoride membranes (GE Healthcare, Piscataway, NJ, USA), and blocked in 5% milk or bovine serum albumin (2%). Blots were incubated with the following primary antibodies: PI16 (1:750, R&D Systems AF4929) and α-Tubulin (1:2000, Cell Signaling 2144S). Following incubation with HRP-conjugated secondary antibodies (Jackson Laboratories), Enhanced chemiluminescent agent (GE Healthcare, Piscataway, NJ, USA) or Clarity Western ECL Substrate (Bio-Rad, Hercules, CA, USA) was used to detect signal. Images were captured on a LAS4000 chemiluminescence system. Band density was determined using LAS Image Quant software (GE Healthcare, Piscataway, NJ, USA).

2.5. Real-Time Quantitative PCR

Relative expression of *Pi16* mRNA in the sciatic nerve and DRG 3 days post CFA treatment and relative mRNA expression levels of cytokines/chemokines, and inflammatory markers in the DRG and hindpaw were quantified using RT-qPCR. Snap-frozen hindpaws were homogenized and RNA extracted using Trizol followed by chloroform/isopropanol extraction according to the manufacturer’s instructions. RNA pellets were resuspended in

DEPC-treated water and used for cDNA amplification using a high-capacity cDNA reverse transcription kit (Applied Biosystems, Waltham, MA) according to the manufacturer's instructions. qPCR was performed on an Applied Biosystems ViiA using TaqMan primers (Integrated DNA Technologies, Coralville, IA, USA). Primers used were: Mouse *Pi16* (IDT, Mm.PT.58.88467939 and Mm.PT.58.22010817). *Cd4* (Mm.PT.58.12602035), *Cd8* (Mm.PT.58.29971442), *Itgam*/*Cd11b* (Mm.PT.58.14195622), *Il10* (Mm.PT.58.13531087), *Il10r* (Mm.PT.58.11980819), *Ccl2* (Mm.PT.58.42151692), *Cxcl12* (Mm.PT.58.32677664), *Il6* (Mm.PT.58.10005566), *Il13* (Mm.PT.58.31366752), *Il1b* (Mm.PT.58.41616450), *Tnfa* (Mm.PT.58.12575861), *Mpo* (Mm.PT.58.33484266), *Il22/Iltifb* (Mm.PT.58.44024580.g), *Il23a* (Mm.PT.58.10594618.g), *Cd3* (Mm.PT.58.42846133), *Ifng* (Mm.PT.58.41769240) and *Ly6g* (Mm.PT.58.30498043).

2.6. Mouse tissue collection and processing

Sciatic nerves, L3-L5 DRGs and hindpaws were collected from mice perfused with 10 mL of chilled 1X PBS, followed by 10 mL 4% paraformaldehyde (PFA) in 1X PBS. Tissues were collected and post-fixed in 4% PFA in 1X PBS for 48 hours. Hindpaws subsequently underwent decalcification in 10% EDTA in water for 14 days. After fixation/decalcification, tissues were cryoprotected in 30% sucrose in water and embedded and frozen in a 1:1 blend of optimal cutting temperature compound (OCT; Bayer Corporation) and 30% sucrose in water. Sciatic nerves and DRGs used for PI16 protein expression, blood-nerve barrier permeability, and leukocyte infiltration were sectioned at 14 μm. DRGs and hindpaws stained for macrophage infiltration were sectioned at 30 μm.

2.7. Human tissue recovery and RNAscope assay

All human tissue recovery procedures were approved by the Institutional Review Boards at the University of Texas at Dallas. Human lumbar DRGs were recovered from organ donors through a collaboration with the Southwest Transplant Alliance, as described previously (Shiers, Sankaranarayanan et al. 2021, Shiers, Sahn et al. 2023). Upon removal, the DRGs were frozen by covering them completely with powdered dry ice and stored in a −80°C freezer. DRG donor information is provided in Supplemental Table 1. Tissues were gradually embedded in OCT in a cryomold by adding small volumes of OCT over dry ice to avoid thawing. All tissues were sectioned at 20 μm onto SuperFrost Plus slides. 3 sections from each donor were collected for experimental probe use in addition to 2 sections for examining tissue quality with positive control and negative control probes for RNAscope. Slides were removed from the cryostat and immediately transferred to cold 10% formalin (4°C; pH 7.4) for 15 minutes. The tissues were then dehydrated in 50% ethanol (5 min), 70% ethanol (5 min), 100% ethanol (5 min), 100% ethanol (5 min) at room temperature. The slides were air dried briefly and then boundaries were drawn around each section using a hydrophobic pen (ImmEdge PAP pen, Vector Labs). When hydrophobic boundaries had dried, RNAscope *in situ* hybridization multiplex fluorescent v2 assay was performed per Advanced Cell Diagnostics protocol as previously described (Ray, Shiers et al. 2023). A 2-minute protease IV digestion time was used for experiments and Akoya fluorescein, Cy3, and Cy5 dyes were used. The probes used were: *PI16* (ACD Cat. 569181), *COL1A2* (ACD Cat. 432721-C2), *PECAM1* (ACD Cat. 487381-C3) and *GFRA2* (ACD Cat. 463011-C3). Following RNAscope, slides were incubated with DAPI (1:5000; Cayman Chemical; Cat

14285) diluted in 0.1M PB at room temperature. Slides were then washed in 0.1M PB, air dried and coverslipped with Prolong Gold Antifade reagent. Imaging was done on an Olympus FV3000 confocal microscope as previously described (Shiers, Sankaranarayanan et al. 2021, Shiers, Sahn et al. 2023). Large diffuse structures or signal that autofluoresced in all 3 channels was determined to be lipofuscin and was not considered true signal (marked in Fig. 7 as white arrowheads). *PI16* quantification was performed on 2–3 images per donor (total of 6 donors). The presence of peri-neuronal *PI16* was analyzed on a total of 566 neurons. Raw values can be found in Supplemental Table 2.

2.8. Mouse immunohistochemistry

Sections were washed in 0.3% Triton-X-100 in PBS, blocked with normal donkey serum (5%), bovine serum albumin (BSA; 2%), and saponin (0.1%), stained with primary antibodies followed by conjugated secondary donkey or goat antibodies (Invitrogen, Grand Island, NY). Primary antibodies used: PI16 (1:75, R&D Systems AF4929), GLUT1 (1:100, Abcam ab652), CD45 (1:50, BD Biosciences 550539), Col14a1 (1:200, Novus, NBP2–15940), CD206 (1:500, Cell Signaling, E6T5J) and CD68 (1:250, Bio-Rad, MCA1957). After washing off unbound secondary antibody, sections were incubated for 30 minutes with DAPI (1 μg/ml). For negative controls, the primary antibody was excluded. For immunostaining, n values represent biological replicates, i.e., tissues processed and stained from individual mice. To determine the mean intensity of fluorescence and the percent area of positive staining, Nikon NIS Elements or NIH ImageJ software was used as previously described (Nichols, Crelli et al. 2021, Balogh, Zhang et al. 2022).

2.9. Flow cytometry

Flow cytometric analysis of DRG leukocytes was carried out as described previously (Singh, Krukowski et al. 2022). Briefly, lumbar DRG (L4–6) were collected 3–15 days after intraplantar CFA injection. Tissue was digested for 20 minutes with gentle agitation with 1.6 mg/ml collagenase in RPMI with 10 mM HEPES and 5 mg/mL BSA at 37°C. The cell suspension was passed through a 70 μm cell strainer and resuspended in 1 mL of RPMI medium supplemented with 10% heat-inactivated FBS and penicillin, streptomycin and L-glutamine. Cells were incubated with live/dead fixable cell dye followed by surface staining using antibodies directed against CD45 Brilliant Violet 570 (BioLegend, clone 30-F11), F4/80 PB (BioLegend, clone BM8) CD11c BV421 (BioLegend, clone N418) and CD206 AF700 (BioLegend, clone 53–6.7) for 30 minutes at 4°C. Cells were resuspended in wash buffer and acquired on Gallios flow cytometer (Beckman Coulter) at the University of Texas MD Anderson Cancer Center Flow Cytometry & Cellular Imaging Core Facility.

2.10. Blood-nerve Barrier Permeability Assay

Vascular permeability of the sciatic nerve endothelium in the sciatic nerve was assessed using a mixture of sodium fluorescein and Evans Blue Albumin (Wick, Harral et al. 2018). Sodium fluorescein (40 mg/kg, i.v.) and Evans Blue Albumin (50 mg/kg, i.v.) were injected on day 3 after intraplantar CFA injection and allowed to circulate for 1 hour. Mice were perfused with 10 mL ice-cold PBS with heparin (5 units/mL) intracardially, and nerves were collected and processed for fluorescent immunohistochemistry as described above. Nerve cross-sections were visualized using an EVOS fluorescence microscope, and the

mean fluorescence intensity quantified and the percent area positive calculated using NIH ImageJ software.

2.11. RNA extraction, library preparation for sequencing, and bulk RNA-seq analysis:

Mice were perfused intracardially with 10-mL ice-cold PBS and lumbar DRGs (L3–5) and overlying meninges were collected. DRGs were collected 3 days post CFA/PBS intraplantar injections. RNA was extracted using the RNeasy MinElute Cleanup Kit (Qiagen, Hilden, Germany), based on the manufacturer's protocol, as described previously (Singhmar, Trinh et al. 2020). The prepared samples were then shipped on dry ice and the bulk RNA sequencing (mRNA library preparation) was performed by Novogene (California, USA; California Clinical Laboratory License No: 05D2146243), after ensuring the samples met or exceeded the proper quality control criteria (Agilent 2100 RNA integrity number for all samples >7). Raw reads in FASTQ format were analyzed using the FastQC tool for quality control (Andrews 2010). The STAR package was used for the reference genome mapping with the mouse genome (mm10) (Dobin and Gingeras 2015). The gene counts were estimated from uniquely mapped reads using the feature Counts program from the Subread tool (Liao, Smyth et al. 2013). Further, the gene counts were normalized and differentially expressed genes (adjusted p-value < 0.05) between wild-type and *Pi16*$^{-/-}$ mice were calculated using the DEseq2 program (Love, Huber et al. 2014). The pathway enrichment analysis was performed using the IPA tool with default parameters.

2.12. Statistical analysis

Data represented as mean ± SEM and was analyzed using GraphPad Prism 9. For Western blots, RT-qPCR, and immunostaining data, statistical analysis was carried out using Student's *t* test; two-way repeated measures ANOVA followed by Šidák analysis was used to analyze von Frey and Hargreaves behavior data and hindpaw edema. A *P* value less than 0.05 was considered statistically significant. Behavioral experiments were carried out over at least two experimental cohorts. For IHC, at least three independent technical replicates were taken from different sections of the same tissue that were stained/imaged together for consistency. We performed Western blot and IHC analyses in female experimental mice only due to the sex differences observed in pain behavioral data.

3. Results

3.1. *Pi16* knockout mice are protected against CFA-induced persistent inflammatory pain hypersensitivity

To identify the role of PI16 in persistent inflammatory pain, we injected complete Freund's adjuvant (CFA, intraplantar) in the hind paws of WT and *Pi16*$^{-/-}$ mice. Baseline mechanical sensitivity was not affected by genetic deletion of *Pi16*. CFA-induced mechanical hypersensitivity lasted for ≥2 weeks in female WT mice (Fig. 1A). We opted to use n=3 WT and *Pi16*$^{-/-}$ for intraplantar injection, since no hypersensitivity was expected in these treatment groups. There were no significant differences in mechanical sensitivity (Fig. 1A) or thermal sensitivity (Fig. 1B) between WT and *Pi16*$^{-/-}$ on day 1 post-CFA. However, *Pi16*$^{-/-}$ mice returned to pre-injection levels of mechanical and thermal sensitivity by days 3–4 post-CFA (Fig. 1B), indicating that deletion of *Pi16* protects against persistent

inflammatory pain hypersensitivity in female mice. No significant differences in baseline paw thickness or CFA-induced paw edema were observed up to 72 h post-CFA (Fig. 1C).

As with females, male *Pi16*$^{-/-}$ mice developed acute mechanical (Fig. 1D) and thermal (Fig. 1E) hypersensitivity post-CFA, and CFA-induced paw edema was unaffected (Fig. 1F). Sexual dimorphism emerged in male mice following CFA injection (Fig. 1 D–F). Mechanical sensitivity in *Pi16*$^{-/-}$ mice recovered rapidly on days 3 and 5 post-CFA, as was seen in females (Fig. 1D). However, from days 7–21, *Pi16*$^{-/-}$ males that received CFA showed a gradual return to mechanical hypersensitivity, becoming significantly more sensitive than their wild-type counterparts on days 16 and 21 post-CFA. A similar timeframe of 'relapse' into thermal hypersensitivity was seen in male *Pi16*$^{-/-}$ mice following CFA (Fig. 1E).

We extended these findings by generating an inducible beta-actin-driven *Pi16*$^{-/-}$ mouse, allowing us to exclude any developmental abnormalities as the cause of the blunted response to CFA in *Pi16*$^{-/-}$ mice. We first validated that tamoxifen treatment reduced expression of PI16 in DRG (Fig. S1). In females (Fig. 2A) and males (Fig. 2B), sustained CFA-induced mechanical hypersensitivity was intact in Cre-ER positive animals that received vehicle. Tamoxifen treatment of wild-type (Cre-ER negative) littermates prior to CFA had no discernable effect on CFA hypersensitivity. Induction of Cre-ER in females and males (Fig. 2A–B) phenocopied the acute pain hypersensitivity and rapid recovery seen in the germline *Pi16*$^{-/-}$ mouse. We saw similarly rapid recovery after CFA in male and female mice where *Pi16* was inducibly deleted only from *Col1a2*$^{+}$ fibroblasts (Fig. 2C–D, combined data for both sexes depicted in Fig. 2E). Collectively, these data indicate a requirement for fibroblast PI16 function in pain hypersensitivity due to hindpaw inflammation.

3.2. PI16 is detected in the Col14a1 fibroblast subset in sciatic nerve epineurium/perineurium

We previously showed that PI16 protein is expressed in sciatic nerve epineurial/perineurial fibroblasts (Singhmar, Trinh et al. 2020). Immunofluorescence analysis shows that PI16 is detectable in sciatic nerve epineurium/perineurial fibroblasts in WT mice on days 1 and 3 post-CFA (Fig. 3A–B). Immunofluorescence was undetectable in negative control samples where anti-PI16 was omitted (Fig. S2). Despite a significant CFA-induced thickening of the epineurium/perineurium (Fig. 3C) where PI16 expression co-localizes with the fibroblast marker Col14a1 (Fig. 3D), we did not detect changes in total sciatic nerve PI16 protein expression comparing CFA-treated and PBS-injected control mice on days 1 or 3 post-CFA (Fig. 3E–F). We found that PI16 also colocalizes with Col14a1 in the sciatic nerve epineurium/perineurium in control PBS-treated mice. The CFA-induced increase in epineurium thickness was populated by PI16 positive fibroblasts. These CFA induced epineurial/perineurial fibroblasts were predominantly Col14a1-positive and co-localized with PI16. The 3D orthogonal slice views confirm co-localization of PI16 and Col14a1 in sciatic nerves. Importantly, though Col14a1 immunoreactivity is seen in the sciatic nerve endoneurium trunk, this staining does not colocalize with PI16 (Fig. S3), confirming our prior findings that PI16 is not expressed on peripheral nerve axons(Singhmar, Trinh et al. 2020).

3.3. CFA does not affect blood-nerve barrier permeability or inflammation in the sciatic nerve

Following nerve injury, PI16 increases blood-nerve barrier permeability with associated leukocyte infiltration (Singhmar, Trinh et al. 2020). To determine whether CFA-induced inflammatory pain was associated with PI16-dependent blood-nerve barrier permeability changes, we intravenously administered sodium fluorescein (Fig. 4A) and Evans Blue albumin (Fig. 4B). Our results show that CFA does not significantly alter permeability to these molecules 72h post-injection, suggesting that PI16 does not cause persistent pain post-CFA by modulating blood-nerve barrier integrity. Consistent with these observations, qPCR of sciatic nerves 72h after CFA did not detect any changes in T-cell or myeloid cell markers compared to controls (Fig. 4C). Furthermore, we did not detect changes in selected cytokine/chemokine expression due to deletion of *Pi16* or CFA injection (Fig. 4D).

3.4. CFA does not affect DRG PI16 expression or leukocyte density

We previously showed that PI16 protein is expressed by DRG meningeal fibroblasts (Singhmar, Trinh et al. 2020). Using immunofluorescence (Fig. 5A) and Western blotting (Figs. 5B–C), we show that there are no significant changes in total DRG PI16 expression at 24h or 72h post-CFA. We also showed previously that PI16 deficiency reduced SNI-induced macrophage infiltration of the DRGs and nerves following spared nerve injury (Singhmar, Trinh et al. 2020). Immunofluorescence analysis showed that the resolution of CFA-induced mechanical allodynia in PI16-deficient female mice at day 3 post-CFA was not associated with statistically significant differences in the number of lumbar DRG parenchymal $CD45^+$ cells compared to PBS-injected controls (Fig. 6A–B). Furthermore, no difference in myeloid cell marker *Cd11b* expression was detected using qPCR (Fig. 6C). Fig. S4 shows no inflammatory molecular changes in DRG/spinal cord between WT and $Pi16^{-/-}$ mice via qPCR. Flow cytometry analysis of DRG also showed no significant differences in the number of $CD45^+$ cells between WT and $Pi16^{-/-}$ mice, at baseline or at 3, 8 and 15 days following CFA injections (Fig. 6D). Finally, qPCR did not detect changes in selected chemokine levels or lymphoid/myeloid cell markers (Fig. 6E).

3.5. PI16 is expressed by human DRG macrophages and fibroblasts

To assess the expression pattern and cell types responsible for *PI16* expression in humans, we performed RNAscope *in situ* hybridization on lumbar L4/5 DRG from male and female human donors (Fig. 7). *PI16* mRNA expression was abundant in non-neuronal cells surrounding neuronal somata (Fig. 7A, B). A subset of $COL1A2^+$ fibroblasts were also $PI16^+$ (Fig. 7A, B), though the vascular endothelial marker PECAM-1 did not overlap with *PI16* mRNA signal. Although PI16 was observed throughout the human DRG, we observed some peri-neuronal PI16 expression, particularly surrounding *GFRA2+* neurons (Fig. 7C). Our quantification shows that nearly 20% of all neurons have peri-neuronal PI16 and among *GFRA2+* neurons, 10% of those have peri-neuronal PI16 expression (Fig. 7D). Collectively, this indicates that *PI16* mRNA is expressed in human sensory ganglia in a subset of fibroblasts and cells surrounding neurons.

3.6. Bulk RNA-seq reveals an increased DRG myeloid cell signature in Pi16$^{-/-}$ mice post-CFA

To better understand the CFA-induced signaling events and gene expression changes in *Pi16*$^{-/-}$ mouse lumbar DRG relative to WT DRG, we performed bulk RNA-sequencing 3 days after hindpaw CFA injection (n=4 biological replicates per condition, Fig. 8A–D). 35 genes were differentially expressed in WT versus *Pi16*$^{-/-}$ DRGs after PBS injection, whereas 92 differentially-expressed genes were identified in WT versus *Pi16*$^{-/-}$ DRGs after CFA (Fig. 8A and Supplemental Table 3). Twenty-one of these genes were shared across PBS and CFA injection (Fig. 8B), leaving 71 differentially-expressed genes unique to CFA injection in *PI16*$^{-/-}$ versus WT (Fig. 8C). The outcomes are in line with previous studies where a number of differentially expressed genes, including *Anxa1* (da Silva, da Silva Cavalcante et al. 2021), *Chil3*, *Camp*, *Ly6c2* (Dietrich, Heinz et al. 2022), *Hck* (Priceputu, Cool et al. 2021), *Itgal* (Li, Wu et al. 2022), *Itgam* (Hegde, Leader et al. 2021), *Itgb2*, *Itgb7* (Bayik, Bartels et al. 2022), *Lcn2* (Huang, Li et al. 2020), *Mmp9*, *Mpo*, *Ncf1* (Sanchez-Pino, Dean et al. 2021), *Mki67* (Liechtenstein, Perez-Janices et al. 2014), *Mmp8* (Marvel and Gabrilovich 2015), *Selplg* and *Csf3r* (Alshetaiwi, Pervolarakis et al. 2020) were associated with anti-inflammatory myeloid cells. Correspondingly, pathway analysis showed the most significant increases in myeloid cell-related pathways (e.g., neutrophil degranulation, neutrophil activation involved in immune response, neutrophil mediated immunity, regulation of neutrophil degranulation, granulocyte migration, positive regulation of myeloid leukocyte mediated immunity; Fig. 8D).

3.7. Neutralization of extracellular PI16 in the DRG/spinal cord accelerates recovery from CFA-induced pain hypersensitivity

Since deletion of PI16 appeared to affect the DRG inflammatory microenvironment following CFA injection, we evaluated the contribution of spinal/DRG PI16 to the onset of CFA-induced inflammatory pain (Fig. 9). We intrathecally injected PI16-blocking antibody or an IgG isotype control antibody in WT female mice. We show that regardless of antibody treatment, mice develop acute mechanical hypersensitivity up to day 4 following CFA injection. From 7 days post-injection, mice that received PI16 neutralizing antibody show greater recovery from CFA-induced hypersensitivity, indicating that WT mice treated with PI16 blocking antibody are protected from transitioning into more persistent CFA-induced mechanical hypersensitivity.

3.8. Increased CD206^{hi} myeloid cells in Pi16$^{-/-}$ mice drive accelerated recovery from CFA pain

Since lumbar DRG bulk-RNA sequencing detected increased levels of transcripts associated with anti-inflammatory myeloid cells in *Pi16*$^{-/-}$ mice after CFA injection (Fig. 8), we analyzed the levels of these cells in *Pi16*$^{-/-}$ and WT DRGs. Flow cytometry detected a strong tendency towards increased numbers of F4/80^{+} CD206^{+} CD11c^{-} macrophages in male, but not female DRG at baseline (Fig. 10A). 3 days after CFA injection in female mice (Fig. 10B), the pan-macrophage marker CD68 showed no significant difference in density in DRG parenchyma or its surrounding meninges (Fig. 10C). There was a significant increase in DRG meningeal CD206^{hi} cell density with no significant change in the *Pi16*$^{-/-}$ DRG

parenchyma (Fig. 10D). This indicates that the acute recovery from CFA injection seen in *Pi16*$^{-/-}$ mice is associated with increased DRG meningeal CD206^{hi} cell density.

To test for a contribution of these CD206^{hi} cells to accelerated recovery from CFA in *Pi16*$^{-/-}$ mice, we depleted CD206^{+} cells using intrathecal injection of mannosylated clodronate liposomes (Niehaus, Taylor-Blake et al. 2021), prior to CFA injection in the hindpaw (Fig. 10E). As expected, *Pi16*$^{-/-}$ mice that received control ('Lip-Empty') liposomes showed the typical accelerated recovery from CFA-induced hypersensitivity. WT mice that received empty liposomes exhibited sustained pain hypersensitivity post-CFA, which showed a tendency towards being augmented in WT mice that received mannosylated clodronate liposomes. In *Pi16*$^{-/-}$ where CD206^{+} cells were depleted, the CFA-induced response was now identical to WT mice treated with control liposomes, showing significantly greater hypersensitivity than *Pi16*$^{-/-}$ controls from 7–15 days post-CFA.

Since CD206^{+} macrophages are known to express IL-10 (Wright, McDonald et al. 2021) and we have previously shown that IL-10-producing macrophages promote resolution of transient inflammatory hyperalgesia (Willemen, Eijkelkamp et al. 2014), we treated a cohort of *Pi16*$^{-/-}$ mice intrathecally with an IL-10 neutralizing antibody after CFA injection. This also attenuated the rapid recovery from CFA-induced hypersensitivity (Fig. 10F).

In order to assess the fibroblast-dependence of the *PI16*$^{-/-}$ CD206^{hi} phenotype, we used inducible, fibroblast-specific *Pi16*$^{-/-}$ mice to assess CD68^{+} and CD206^{hi} density in lumbar DRGs from CFA-injected mice that had received either prior vehicle or tamoxifen (Fig. 11). Consistent with mice with germline deletion of *Pi16* (Fig. 10B–D), tamoxifen-induced deletion of *Pi16* from fibroblasts was associated with no significant change in CD68 density (Fig. 11A, B), but a significant increase in CD206^{hi} staining density (Fig. 11A, C). Collectively, these data suggest that fibroblast-derived PI16 drives increased abundance of an anti-inflammatory, CD206^{hi} macrophage population in the lumbar DRG meninges of female *Pi16*$^{-/-}$ mice and may contribute to their accelerated recovery from inflammatory pain.

3.9. Pi16$^{-/-}$ mice show reduced skin macrophage density and increased CD206 post-CFA

Based on the phenotypic differences in macrophages detected in *Pi16*$^{-/-}$ lumbar DRGs (Figs. 10–11), we evaluated PI16 expression alongside myeloid and lymphoid cell marker expression in hindpaw skin post-CFA (Fig. 12A). *Pi16* expression did not significantly change in WT female mice post-CFA, nor was this associated with increased CD11b (*Itgam*) expression compared to *Pi16*$^{-/-}$ mice. CD4 and CD8 expression significantly increased in *Pi16*$^{-/-}$ mice, though this did not occur until the latter stages of the CFA response (21d post-injection). qPCR for pro-inflammatory cytokine gene expression did not yield any significant differences between WT and *Pi16*$^{-/-}$ mice apart from CD3 and interferon gamma on day 8 post CFA-injection (Fig. S5). IHC of female hindpaw skin 3d post-CFA revealed a significantly lower density of CD68^{+} macrophages in the skin of *Pi16*$^{-/-}$ mice, and a significant increase in CD206^{hi} labeling (Fig. 12B–C), consistent with our observations in lumbar DRG meninges (Fig. 10). This reduced CD68^{+} and augmented CD206^{hi} accumulation was mirrored in hindpaw tissues from the inducible fibroblast-specific *Pi16*$^{-/-}$ (Fig. 12D–E). This is indicative of a similar anti-inflammatory

shift in macrophage phenotype at the site of inflammation at a timepoint where *Pi16*$^{-/-}$ mice exhibit recovery from cutaneous hypersensitivity.

4. Discussion

Our findings provide evidence for a role of the putative protease inhibitor PI16 in CFA-induced inflammatory pain. PI16 has been shown by our group and others to be expressed by neural tissue-associated fibroblasts (Singhmar, Trinh et al. 2020, Wolbert, Li et al. 2020). We show that deletion of PI16 either systemically or from fibroblasts alone reduces the duration and degree of mechanical and heat hypersensitivity following CFA. Bulk RNA sequencing of DRG innervating CFA-injected hindpaws revealed upregulation of myeloid cell-related GO processes in *Pi16*$^{-/-}$ mice. We also show that PI16 deletion is associated with a net increase in alternatively activated, CD206^{hi} macrophages in the skin and DRG meninges after induction of inflammation. Accordingly, the accelerated recovery from CFA-induced nociception is dependent on spinal IL-10 signaling. Taken together, these data suggest that PI16^{+} fibroblasts significantly modulate the anti-inflammatory milieu at sites of inflammation and the associated DRGs, thereby determining the severity and duration of inflammatory pain.

Previously, we characterized the central role of PI16 in spared nerve injury, where we found that PI16 secretion by fibroblasts in the meninges of the DRG and epineurium/perineurium of the injured nerve was necessary to establish chronic pain. In this nerve injury model, PI16 increased vascular permeability and leukocyte infiltration via phosphorylation of the endothelial barrier protein MLC2 (Singhmar, Trinh et al. 2020). However, there are a multitude of differences in the pathophysiology and mechanisms driving neuropathic and inflammatory pain states (Xu and Yaksh 2011), so we set out to determine the role of PI16 in the hindpaw CFA model of inflammatory pain.

Female PI16 knockout mice showed atypically rapid recovery from intraplantar CFA, recovering normal sensitivity within 24–72 hours of injection. Male mice with germline *Pi16* deletion exhibited a similarly rapid recovery at first, but gradually ‘relapsed’ into tactile and thermal hypersensitivity at around 12–14 days post-CFA. The mechanisms underlying this sex-specific relapse require further study, but it is unlikely that this would have implications for therapeutic targeting of PI16, because of the lack of sexual dimorphism when PI16 was inducibly deleted or blocked with a neutralizing antibody. Importantly, the protective effect of *Pi16* deletion was replicated following inducible systemic and fibroblast-specific deletion of PI16 in adult mice, suggesting that persistent pain following CFA does indeed require PI16 production from fibroblasts. Interestingly, this protection against CFA-induced pain was not associated with deficits in paw edema, suggesting that increased vascular permeability and plasma extravasation are not impacted by PI16 deletion.

In contrast to the SNI neuropathic pain model, we did not detect increased PI16 protein expression in the neuroaxis (sciatic, lumbar DRG) following CFA, despite epi/perineurium thickening in the ipsilateral sciatic nerve. Additionally, we did not observe increased blood-nerve barrier permeability or increased overall leukocyte density or cytokine expression in the DRG, despite the observation that, as with neuropathic pain, female *Pi16*$^{-/-}$ mice

were protected from persistent inflammatory pain. This strongly suggested that a mechanism other than barrier function protects *Pi16*$^{-/-}$ mice from CFA-induced pain. In the absence of detectable changes in PI16 expression, it remains to be established what post-translational modifications PI16 may undergo that modify its function. Additionally, single cell RNAseq analysis of skin fibroblasts suggests PI16 is expressed in a universal fibroblast subtype under steady-state conditions in skin (and elsewhere). Expression of PI16 then decreases as fibroblasts are perturbed and undergo differentiation into more specialized subtypes (Buechler, Pradhan et al. 2021). Such findings would shed light on how a significant change in detectable PI16 need not be necessary to explain the accelerated recovery from CFA-induced inflammation seen in *Pi16*$^{-/-}$ mice.

Bulk RNA sequencing of *Pi16*$^{-/-}$ DRG following CFA revealed increased expression of several genes consistent with increased myeloid cell density. This was also observed histologically in CFA-injected hindpaw skin and associated DRG meninges, but not the DRG parenchyma. The latter observation suggests CD68^{+} macrophages do not accumulate extensively in the DRG when compared to more chronic/neuropathic pain models, such as chemotherapy-induced peripheral neuropathy (Zhang, Li et al. 2016). Prior studies have suggested that anti-inflammatory myeloid cells are important for the resolution of pain hypersensitivity. A spinal CD163^{+} macrophage population was recently identified that increased anti-inflammatory cytokine production and reduced microgliosis following nerve injury (Niehaus, Taylor-Blake et al. 2021). Similarly, we show that the presence of these anti-inflammatory myeloid cells was required for the protective effects of PI16 deletion, since *Pi16*$^{-/-}$ mice were no longer protected from CFA-induced pain if CD206^{+} myeloid cells were depleted beforehand. CD206^{+} macrophages are thought to have anti-fibrotic effects (Kurachi, Kurita et al. 2021). In other tissues, CD206 marks a resident interstitial macrophage population that constitutively produces high levels of chemokines and immunosuppressive cytokines (Schyns, Bai et al. 2019). This would be consistent with our observation that the protective effect of PI16 deletion is IL-10-dependent. Our qPCR data hints at a late-stage elevation in CD4 and CD8 expression which warrants further study, but the timepoints at which this becomes significant (21 days post-CFA) are much later than those where behavioral differences are seen in the *Pi16*$^{-/-}$ post-CFA.

Consequently, we propose that deletion of PI16 from fibroblasts promotes a net accumulation of alternatively activated/M2-like macrophages, resulting in accelerated recovery from inflammatory pain. It remains to be established whether addition of exogenous PI16 to the skin or DRG meninges would promote a net polarization toward or accumulation of classical/M1 macrophage phenotypes, resulting in persistent sensitization and pain. Nevertheless, these data add to the growing appreciation of fibroblasts as modulators of pain via immunomodulation (Shinotsuka and Denk 2022). For example, the anti-fibrotic drug Nintedanib reduced pro-fibrotic cytokine secretion by human M1 macrophages and reduced the synthesis of M2a markers such as CD206 (Zhang, Ayaub et al. 2020).

Our data raise interesting questions about the contribution of fibroblasts to inflammatory pain in male versus female mice. Further work is needed to characterize macrophage composition of skin and DRG beyond 3 days post-CFA, but the behavioral data suggest

that boosting M2-like macrophage numbers within this early window can have lasting effects. The observation that female *Pi16*$^{-/-}$ mice remain protected from sustained pain, whereas males exhibit a 'relapse' into hypersensitivity suggests there is sexual dimorphism in the response to CFA, in the requirement for PI16, CD206 and/or IL-10 expression in inflammatory pain. Importantly, this difference is absent in male inducible fibroblast-specific *Pi16*$^{-/-}$ mice, suggesting that the factors responsible for this relapse effect lie outside of fibroblasts. Though further study is required, the immune system is a promising candidate since there is known PI16 expression by regulatory T cells (Nicholson, Mavrangelos et al. 2012, Becker, Dedden et al. 2021, Schweda, Becker et al. 2022). This would be consistent with several reports that ascribe sexual dimorphism in pain behaviors to differences in immune system function (Sorge, Mapplebeck et al. 2015, Rosen, Ham et al. 2017).

We saw a strong tendency toward reduced overall CD68^{+} macrophage density in *Pi16*$^{-/-}$ mice compared to wild-type at sites of inflammation. These observations are consistent with the loss of PI16 impairing endothelial migration of immune cells, as we described previously (Singhmar, Trinh et al. 2020). On the other hand, we cannot exclude an effect of PI16 on macrophage phenotype or bias in M1/M2 chemotaxis at this stage. The mechanisms linking fibroblast PI16 to macrophage phenotype remain to be established. However, it is well-established in other organs and disease models that macrophages receive differentiation and phenotypic cues from surrounding stromal cells such as fibroblasts (Bellomo, Gentek et al. 2021). Others have observed that conditioned media from activated fibroblasts increased macrophage iNOS and CD86 expression and reduced arginase I and CD206 expression in alveolar macrophages *in vitro*, an effect ascribed largely to fibroblast-derived CXCL10 (Tsai, Chen et al. 2019).

Additional experiments are required to address whether the effect of PI16 deletion on macrophage phenotype is constitutive, or manifests only in response to an inflammatory insult. Our data suggest a tendency toward increased CD206^{hi} and reduced overall macrophage density at baseline, prior to CFA injection, but this does not reach statistical significance in most instances. Our data suggest that such an increase in CD206^{hi} cells does not promote loss of sensitivity at baseline, but is able to dampen hypersensitivity following CFA injection. The directionality of the phenotypic difference induced by deletion of PI16 awaits determination – i.e., does reduced CD68^{+} cell accumulation generate a milieu in which CD206^{hi} cells become more abundant, or does increased CD206^{hi} cell density dampen inflammation and reduce CD68^{+} cell accumulation? Certainly, fibroblasts are capable of secreting mediators such as TSG-6 and COX-2 metabolites that promote M2-like macrophage polarization (Ferrer, Saalbach et al. 2017). An additional possibility is that MMP2, which is normally inhibited by PI16 (Hazell, Peachey et al. 2016) becomes unconstrained in the absence of PI16, thereby promoting M2-like macrophage polarization, an effect that was ascribed to MMP2 activity in melanoma models (Muniz-Bongers, McClain et al. 2021). Further work is needed to determine the mechanisms involved.

Taken together, our findings support a model in which PI16 deletion promotes CD206^{hi} macrophage accumulation in the skin and DRG to accelerate recovery from inflammatory pain. Given that our prior observations on the role of PI16 in neuropathic pain have now been extended to inflammatory pain, we contend that PI16 continues to represent an

attractive non-neuronal target for pain management, with conserved expression in the human DRG.

Supplementary Material

Refer to Web version on PubMed Central for supplementary material.

Acknowledgements

This work was funded by R01NS116704 (to CJH, AJS, TJP, EEU) and a Rita Allen Foundation Award in Pain (to AJS). The flow cytometry carried out in this project was supported by the MD Anderson Cancer Center Support Grant from NIH/NCI under award number P30CA016672. We wish to thank Drs. Jenolyn Alexander and James Nichols for technical assistance with microscopy and image quantification.

Data availability

All datasets will be made available upon request.

Abbreviations:

CFA	Complete Freund's Adjuvant
DRG	Dorsal root ganglion
EDTA	Ethylenediaminetetraacetic acid
PBS	Phosphate-buffered saline
PFA	Paraformaldehyde
PI16	Protease Inhibitor 16
PWL	Paw withdrawal latency
PWT	Paw withdrawal threshold
TAM	Tamoxifen
WT	Wild-type

References

Alshetaiwi H, Pervolarakis N, McIntyre LL, Ma D, Nguyen Q, Rath JA, Nee K, Hernandez G, Evans K, Torosian L, Silva A, Walsh C and Kessenbrock K (2020). "Defining the emergence of myeloid-derived suppressor cells in breast cancer using single-cell transcriptomics." Sci Immunol 5(44).

Andrews S (2010). "A quality control tool for high throughput sequence data.", from http://www.bioinformatics.babraham.ac.uk/projects/fastqc/.

Balogh M, Zhang J, Gaffney CM, Kalakuntla N, Nguyen NT, Trinh RT, Aguilar C, Pham HV, Milutinovic B, Nichols JM, Mahalingam R and Shepherd AJ (2022). "Sensory neuron dysfunction in orthotopic mouse models of colon cancer." J Neuroinflammation 19(1): 204. [PubMed: 35962398]

Bayik D, Bartels CF, Lovrenert K, Watson DC, Zhang D, Kay K, Lee J, Lauko A, Johnson S, Lo A, Silver DJ, McGraw M, Grabowski M, Mohammadi AM, Veglia F, Fan Y, Vogelbaum MA, Scacheri

P and Lathia JD (2022). “Distinct Cell Adhesion Signature Defines Glioblastoma Myeloid-Derived Suppressor Cell Subsets.” Cancer Res 82(22): 4274–4287. [PubMed: 36126163]

Becker E, Dedden M, Gall C, Wiendl M, Ekici AB, Schulz-Kuhnt A, Schweda A, Voskens C, Hegazy A, Vitali F, Atreya R, Müller TM, Atreya I, Neurath MF and Zundler S (2021). “Residual homing of α4β7-expressing β1(+)PI16(+) regulatory T cells with potent suppressive activity correlates with exposure-efficacy of vedolizumab.” Gut.

Bellomo A, Gentek R, Golub R and Bajénoff M (2021). “Macrophage-fibroblast circuits in the spleen.” Immunol Rev 302(1): 104–125. [PubMed: 34028841]

Buechler MB, Pradhan RN, Krishnamurty AT, Cox C, Calviello AK, Wang AW, Yang YA, Tam L, Caothien R, Roose-Girma M, Modrusan Z, Arron JR, Bourgon R, Müller S and Turley SJ (2021). “Cross-tissue organization of the fibroblast lineage.” Nature 593(7860): 575–579. [PubMed: 33981032]

Chaplan SR, Bach FW, Pogrel JW, Chung JM and Yaksh TL (1994). “Quantitative assessment of tactile allodynia in the rat paw.” Journal of Neuroscience Methods 53(1): 55–63. [PubMed: 7990513]

da Silva SF, da Silva Cavalcante LR, Fonseca Junior EA, da Silva JM, Lopes JC and Damazo AS (2021). “Analysis of the myeloid-derived suppressor cells and annexin A1 in multibacillary leprosy and reactional episodes.” BMC Infect Dis 21(1): 1050. [PubMed: 34627197]

Dahlhamer J, Lucas J, Zelaya C, Nahin R, Mackey S, DeBar L, Kerns R, Von Korff M, Porter L and Helmick C (2018). “Prevalence of Chronic Pain and High-Impact Chronic Pain Among Adults - United States, 2016.” MMWR Morb Mortal Wkly Rep 67(36): 1001–1006. [PubMed: 30212442]

Deng M, Yang S, Ji Y, Lu Y, Qiu M, Sheng Y, Sun W and Kong X (2020). “Overexpression of peptidase inhibitor 16 attenuates angiotensin II-induced cardiac fibrosis via regulating HDAC1 of cardiac fibroblasts.” J Cell Mol Med 24(9): 5249–5259. [PubMed: 32227584]

Dietrich O, Heinz A, Goldmann O, Geffers R, Beineke A, Hiller K, Saliba AE and Medina E (2022). “Dysregulated Immunometabolism Is Associated with the Generation of Myeloid-Derived Suppressor Cells in Staphylococcus aureus Chronic Infection.” J Innate Immun 14(3): 257–274. [PubMed: 34763332]

Dobin A and Gingeras TR (2015). “Mapping RNA-seq Reads with STAR.” Curr Protoc Bioinformatics 51: 11.14.11–11.14.19.

Ferrer RA, Saalbach A, Grünwedel M, Lohmann N, Forstreuter I, Saupe S, Wandel E, Simon JC and Franz S (2017). “Dermal Fibroblasts Promote Alternative Macrophage Activation Improving Impaired Wound Healing.” Journal of Investigative Dermatology 137(4): 941–950. [PubMed: 28017830]

Frost RJ and Engelhardt S (2007). “A secretion trap screen in yeast identifies protease inhibitor 16 as a novel antihypertrophic protein secreted from the heart.” Circulation 116(16): 1768–1775. [PubMed: 17909105]

Hargreaves K, Dubner R, Brown F, Flores C and Joris J (1988). “A new and sensitive method for measuring thermal nociception in cutaneous hyperalgesia.” Pain 32(1): 77–88. [PubMed: 3340425]

Hazell GGJ, Peachey AMG, Teasdale JE, Sala-Newby GB, Angelini GD, Newby AC and White SJ (2016). “PI16 is a shear stress and inflammation-regulated inhibitor of MMP2.” Scientific Reports 6(1): 39553. [PubMed: 27996045]

Hegde S, Leader AM and Merad M (2021). “MDSC: Markers, development, states, and unaddressed complexity.” Immunity 54(5): 875–884. [PubMed: 33979585]

Hope CM, Welch J, Mohandas A, Pederson S, Hill D, Gundsambuu B, Eastaff-Leung N, Grosse R, Bresatz S, Ang G, Papademetrios M, Zola H, Duhen T, Campbell D, Brown CY, Krumbiegel D, Sadlon T, Couper JJ and Barry SC (2019). “Peptidase inhibitor 16 identifies a human regulatory T-cell subset with reduced FOXP3 expression over the first year of recent onset type 1 diabetes.” Eur J Immunol 49(8): 1235–1250. [PubMed: 31127857]

Huang T, Li Y, Zhou Y, Lu B, Zhang Y, Tang D, Gan Y, He Z, Chen Z, Yu W and Li P (2020). “Stroke Exacerbates Cancer Progression by Upregulating LCN2 in PMN-MDSC.” Front Immunol 11: 299. [PubMed: 32153594]

Krukowski K, Eijkelkamp N, Laumet G, Hack CE, Li Y, Dougherty PM, Heijnen CJ and Kavelaars A (2016). “CD8+ T Cells and Endogenous IL-10 Are Required for Resolution of Chemotherapy-Induced Neuropathic Pain.” J Neurosci 36(43): 11074–11083. [PubMed: 27798187]

Kurachi I, Kurita E, Takushima A and Suga H (2021). “Human CD206+ Macrophages Show Antifibrotic Effects on Human Fibroblasts through an IL-6-Dependent Mechanism In Vitro.” Plast Reconstr Surg 147(2): 231e–239e. [PubMed: 33370071]

Li R, Wu X, Xue K and Li J (2022). “ITGAL infers adverse prognosis and correlates with immunity in acute myeloid leukemia.” Cancer Cell Int 22(1): 268. [PubMed: 35999614]

Liao Y, Smyth GK and Shi W (2013). “The Subread aligner: fast, accurate and scalable read mapping by seed-and-vote.” Nucleic Acids Res 41(10): e108. [PubMed: 23558742]

Liechtenstein T, Perez-Janices N, Gato M, Caliendo F, Kochan G, Blanco-Luquin I, Van der Jeught K, Arce F, Guerrero-Setas D, Fernandez-Irigoyen J, Santamaria E, Breckpot K and Escors D (2014). “A highly efficient tumor-infiltrating MDSC differentiation system for discovery of anti-neoplastic targets, which circumvents the need for tumor establishment in mice.” Oncotarget 5(17): 7843–7857. [PubMed: 25151659]

Love MI, Huber W and Anders S (2014). “Moderated estimation of fold change and dispersion for RNA-seq data with DESeq2.” Genome Biol 15(12): 550. [PubMed: 25516281]

Marvel D and Gabrilovich DI (2015). “Myeloid-derived suppressor cells in the tumor microenvironment: expect the unexpected.” J Clin Invest 125(9): 3356–3364. [PubMed: 26168215]

Muniz-Bongers LR, McClain CB, Saxena M, Bongers G, Merad M and Bhardwaj N (2021). “MMP2 and TLRs modulate immune responses in the tumor microenvironment.” JCI Insight 6(12).

Nichols JM, Crelli CV, Liu L, Pham HV, Janjic JM and Shepherd AJ (2021). “Tracking macrophages in diabetic neuropathy with two-color nanoemulsions for near-infrared fluorescent imaging and microscopy.” Journal of Neuroinflammation 18(1): 299. [PubMed: 34949179]

Nicholson IC, Mavrangelos C, Bird DR, Bresatz-Atkins S, Eastaff-Leung NG, Grose RH, Gundsambuu B, Hill D, Millard DJ, Sadlon TJ, To S, Zola H, Barry SC and Krumbiegel D (2012). “PI16 is expressed by a subset of human memory Treg with enhanced migration to CCL17 and CCL20.” Cell Immunol 275(1–2): 12–18. [PubMed: 22533972]

Niehaus JK, Taylor-Blake B, Loo L, Simon JM and Zylka MJ (2021). “Spinal macrophages resolve nociceptive hypersensitivity after peripheral injury.” Neuron 109(8): 1274–1282. [PubMed: 33667343]

Priceputu E, Cool M, Bouchard N, Caceres-Cortes JR, Lowell CA, Hanna Z and Jolicoeur P (2021). “HIV-1 Nef Induces Hck/Lyn-Dependent Expansion of Myeloid-Derived Suppressor Cells Associated with Elevated Interleukin-17/G-CSF Levels.” J Virol 95(17): e0047121. [PubMed: 34106001]

Ray PR, Shiers S, Caruso JP, Tavares-Ferreira D, Sankaranarayanan I, Uhelski ML, Li Y, North RY, Tatsui C, Dussor G, Burton MD, Dougherty PM and Price TJ (2023). “RNA profiling of human dorsal root ganglia reveals sex differences in mechanisms promoting neuropathic pain.” Brain 146(2): 749–766. [PubMed: 35867896]

Reeves JR, Dulude H, Panchal C, Daigneault L and Ramnani DM (2006). “Prognostic value of prostate secretory protein of 94 amino acids and its binding protein after radical prostatectomy.” Clin Cancer Res 12(20 Pt 1): 6018–6022. [PubMed: 17062675]

Reeves JR, Xuan JW, Arfanis K, Morin C, Garde SV, Ruiz MT, Wisniewski J, Panchal C and Tanner JE (2005). “Identification, purification and characterization of a novel human blood protein with binding affinity for prostate secretory protein of 94 amino acids.” Biochem J 385(Pt 1): 105–114. [PubMed: 15344909]

Regn M, Laggerbauer B, Jentzsch C, Ramanujam D, Ahles A, Sichler S, Calzada-Wack J, Koenen RR, Braun A, Nieswandt B and Engelhardt S (2016). “Peptidase inhibitor 16 is a membrane-tethered regulator of chemerin processing in the myocardium.” J Mol Cell Cardiol 99: 57–64. [PubMed: 27539859]

Rosen S, Ham B and Mogil JS (2017). “Sex differences in neuroimmunity and pain.” Journal of Neuroscience Research 95(1–2): 500–508. [PubMed: 27870397]

Sanchez-Pino MD, Dean MJ and Ochoa AC (2021). “Myeloid-derived suppressor cells (MDSC): When good intentions go awry.” Cell Immunol 362: 104302. [PubMed: 33592540]

Schweda A, Becker E, Wiendl M, Atreya R, Atreya I, Müller TM, Neurath MF and Zundler S (2022). “Etrolizumab-s Does Not Induce Residual Trafficking of Regulatory T Cells.” Inflammatory Bowel Diseases 28(11): 1746–1755. [PubMed: 35815779]

Schyns J, Bai Q, Ruscitti C, Radermecker C, De Schepper S, Chakarov S, Farnir F, Pirottin D, Ginhoux F, Boeckxstaens G, Bureau F and Marichal T (2019). “Non-classical tissue monocytes and two functionally distinct populations of interstitial macrophages populate the mouse lung.” Nat Commun 10(1): 3964. [PubMed: 31481690]

Shiers S, Sahn JJ and Price TJ (2023). “MNK1 and MNK2 Expression in the Human Dorsal Root and Trigeminal Ganglion.” Neuroscience.

Shiers SI, Sankaranarayanan I, Jeevakumar V, Cervantes A, Reese JC and Price TJ (2021). “Convergence of peptidergic and non-peptidergic protein markers in the human dorsal root ganglion and spinal dorsal horn.” J Comp Neurol 529(10): 2771–2788. [PubMed: 33550628]

Shinotsuka N and Denk F (2022). “Fibroblasts: the neglected cell type in peripheral sensitisation and chronic pain? A review based on a systematic search of the literature.” BMJ Open Sci 6(1): e100235.

Singh SK, Krukowski K, Laumet GO, Weis D, Alexander JF, Heijnen CJ and Kavelaars A (2022). “CD8+ T cell-derived IL-13 increases macrophage IL-10 to resolve neuropathic pain.” JCI Insight 7(5).

Singhmar P, Trinh RTP, Ma J, Huo X, Peng B, Heijnen CJ and Kavelaars A (2020). “The fibroblast-derived protein PI16 controls neuropathic pain.” Proc Natl Acad Sci U S A 117(10): 5463–5471. [PubMed: 32079726]

Sorge RE, Mapplebeck JC, Rosen S, Beggs S, Taves S, Alexander JK, Martin LJ, Austin JS, Sotocinal SG, Chen D, Yang M, Shi XQ, Huang H, Pillon NJ, Bilan PJ, Tu Y, Klip A, Ji RR, Zhang J, Salter MW and Mogil JS (2015). “Different immune cells mediate mechanical pain hypersensitivity in male and female mice.” Nat Neurosci 18(8): 1081–1083. [PubMed: 26120961]

Tsai CF, Chen JH and Yeh WL (2019). “Pulmonary fibroblasts-secreted CXCL10 polarizes alveolar macrophages under pro-inflammatory stimuli.” Toxicol Appl Pharmacol: 114698. [PubMed: 31394157]

Wick MJ, Harral JW, Loomis ZL and Dempsey EC (2018). “An Optimized Evans Blue Protocol to Assess Vascular Leak in the Mouse.” J Vis Exp(139).

Willemen HL, Eijkelkamp N, Garza Carbajal A, Wang H, Mack M, Zijlstra J, Heijnen CJ and Kavelaars A (2014). “Monocytes/Macrophages control resolution of transient inflammatory pain.” J Pain 15(5): 496–506. [PubMed: 24793056]

Wolbert J, Li X, Heming M, Mausberg AK, Akkermann D, Frydrychowicz C, Fledrich R, Groeneweg L, Schulz C, Stettner M, Alonso Gonzalez N, Wiendl H, Stassart R and Meyer zu Hörste G (2020). “Redefining the heterogeneity of peripheral nerve cells in health and autoimmunity.” Proceedings of the National Academy of Sciences 117(17): 9466.

Wright PB, McDonald E, Bravo-Blas A, Baer HM, Heawood A, Bain CC, Mowat AM, Clay SL, Robertson EV, Morton F, Nijjar JS, Ijaz UZ, Milling SWF and Gaya DR (2021). “The mannose receptor (CD206) identifies a population of colonic macrophages in health and inflammatory bowel disease.” Sci Rep 11(1): 19616. [PubMed: 34608184]

Xu Q and Yaksh TL (2011). “A brief comparison of the pathophysiology of inflammatory versus neuropathic pain.” Curr Opin Anaesthesiol 24(4): 400–407. [PubMed: 21659872]

Yong RJ, Mullins PM and Bhattacharyya N (2022). “Prevalence of chronic pain among adults in the United States.” Pain 163(2): e328–e332. [PubMed: 33990113]

Zhang F, Ayaub EA, Wang B, Puchulu-Campanella E, Li Y-H, Hettiarachchi SU, Lindeman SD, Luo Q, Rout S, Srinivasarao M, Cox A, Tsoyi K, Nickerson-Nutter C, Rosas IO and Low PS (2020). “Reprogramming of profibrotic macrophages for treatment of bleomycin-induced pulmonary fibrosis.” EMBO Molecular Medicine 12(8): e12034. [PubMed: 32597014]

Zhang H, Li Y, de Carvalho-Barbosa M, Kavelaars A, Heijnen CJ, Albrecht PJ and Dougherty PM (2016). “Dorsal Root Ganglion Infiltration by Macrophages Contributes to Paclitaxel Chemotherapy-Induced Peripheral Neuropathy.” J Pain 17(7): 775–786. [PubMed: 26979998]

Zheng B, Zhang Z, Black CM, de Crombrugghe B and Denton CP (2002). “Ligand-dependent genetic recombination in fibroblasts : a potentially powerful technique for investigating gene function in fibrosis.” Am J Pathol 160(5): 1609–1617. [PubMed: 12000713]

Highlights

1. CFA-induced inflammatory pain is markedly reduced in *Pi16*$^{-/-}$ mice.
2. RNA-seq of *Pi16*$^{-/-}$ mouse DRG post-CFA reveals an increased myeloid cell signature.
3. CD206^{hi} macrophages are increased in DRG meninges and paw skin of CFA-injected *Pi16*$^{-/-}$ mice.
4. Ablation of spinal/DRG CD206^{+} macrophages prolongs CFA-induced pain.

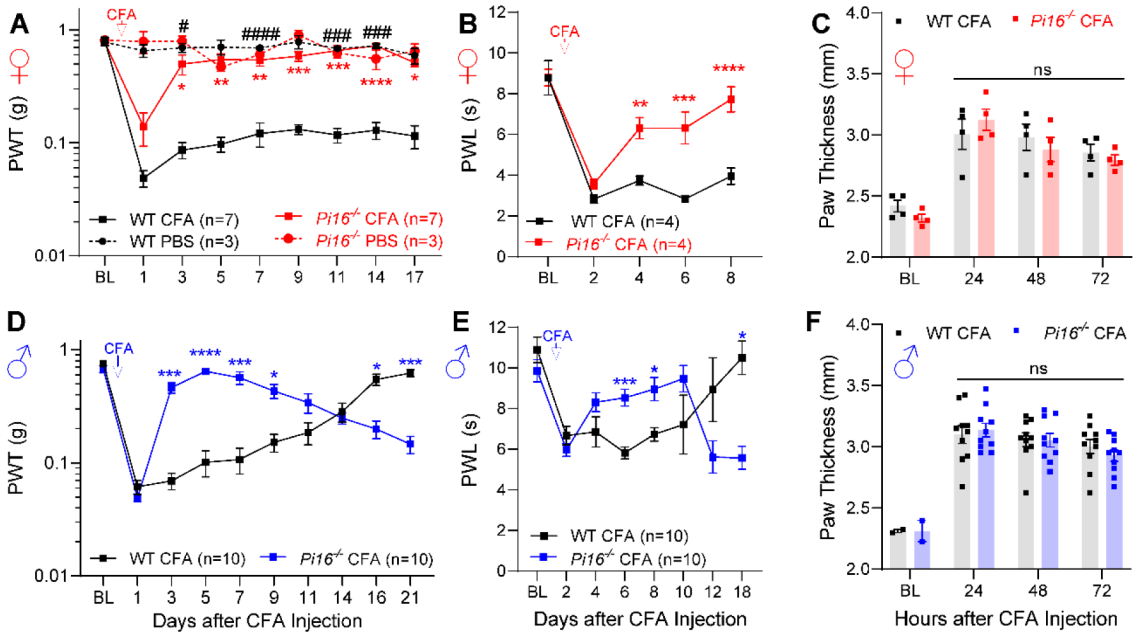

Fig. 1.

Role of *Pi16* deletion in inflammatory pain. (A, D) Inflammatory pain was induced by intraplantar CFA injection. Mechanical allodynia was assessed at baseline and over time using von Frey filaments in female (A) and male (D) mice. Mixed-effects analysis, Šidák's multiple comparisons test: WT CFA vs *Pi16*$^{-/-}$ CFA: *P<0.05, **P<0.01, ***P<0.005, ****P<0.0001, WT PBS vs WT CFA: #P<0.05, ###P<0.01, ####P<0.0001. (B, E) Thermal sensitivity was assessed at baseline and over time in female (B) and male (E) mice using Hargreaves' test. Mixed-effects analysis, Šidák's multiple comparisons test: *P<0.05, **P<0.01, ***P<0.005, ****P<0.0001. (C, F) Hind paw thickness at baseline and over time following intraplantar CFA injection in female (C) and male (F) mice was measured using a Digimatic micrometer. Two-way ANOVA, Šidák's multiple comparisons test.

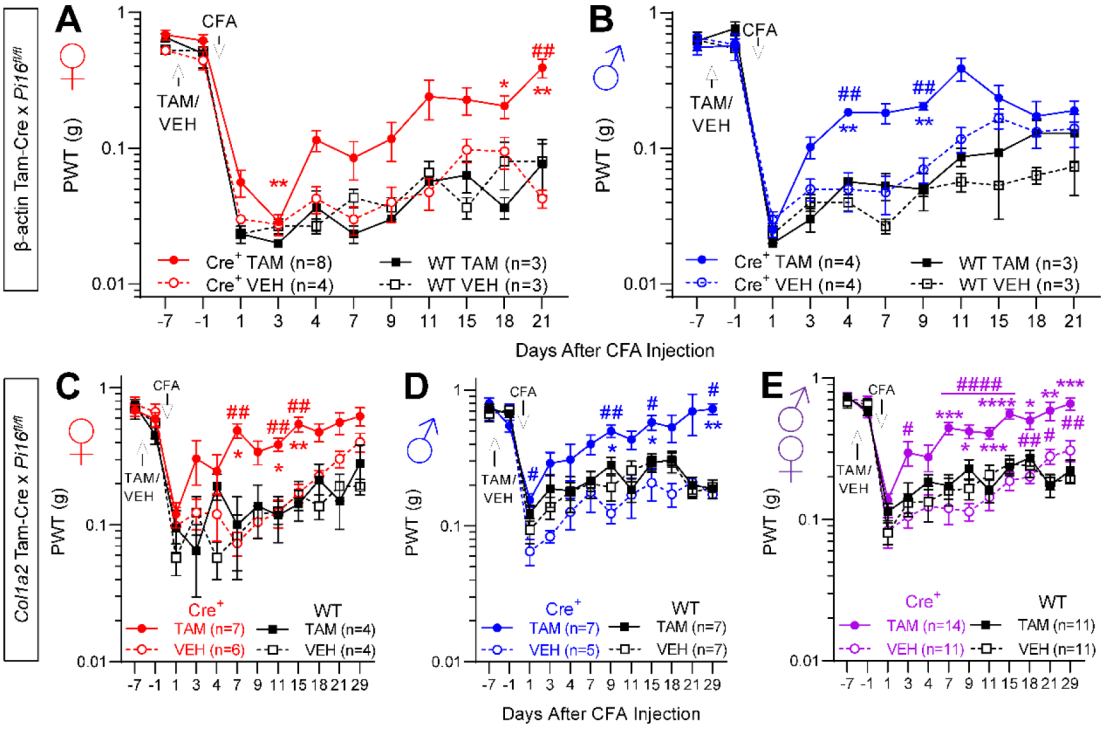

Fig. 2.

Hindpaw von Frey following CFA in systemic inducible *Pi16*$^{-/-}$ (A-B) and fibroblast-specific inducible *Pi16*$^{-/-}$ (C-D). Cre-positive (Cre^{+}) or wild-type littermate controls (WT) were treated with vehicle (VEH) or tamoxifen (TAM) between baseline measurements 1 and 2 (days −7 and −1 relative to intraplantar CFA). (A, B) Systemic inducible deletion of PI16 protects females from acute and prolonged CFA-induced hypersensitivity, whereas males only show attenuation of pain up to 11–15 days post-CFA. (C, D) Inducible deletion of PI16 from *Col1a2* fibroblasts protects female (C) and male (D) mice from prolonged CFA-induced mechanical hypersensitivity. Merged results from (C) and (D) are depicted in panel (E). Two-way repeated-measures ANOVA, Šidák's multiple comparisons tests: Cre^{+} + TAM vs WT + TAM: *P<0.05, **P<0.01, ***P<0.005, ****P<0.0001. Cre^{+} + TAM vs Cre^{+} + VEH: #P<0.05, ##P<0.01, ####P<0.0001.

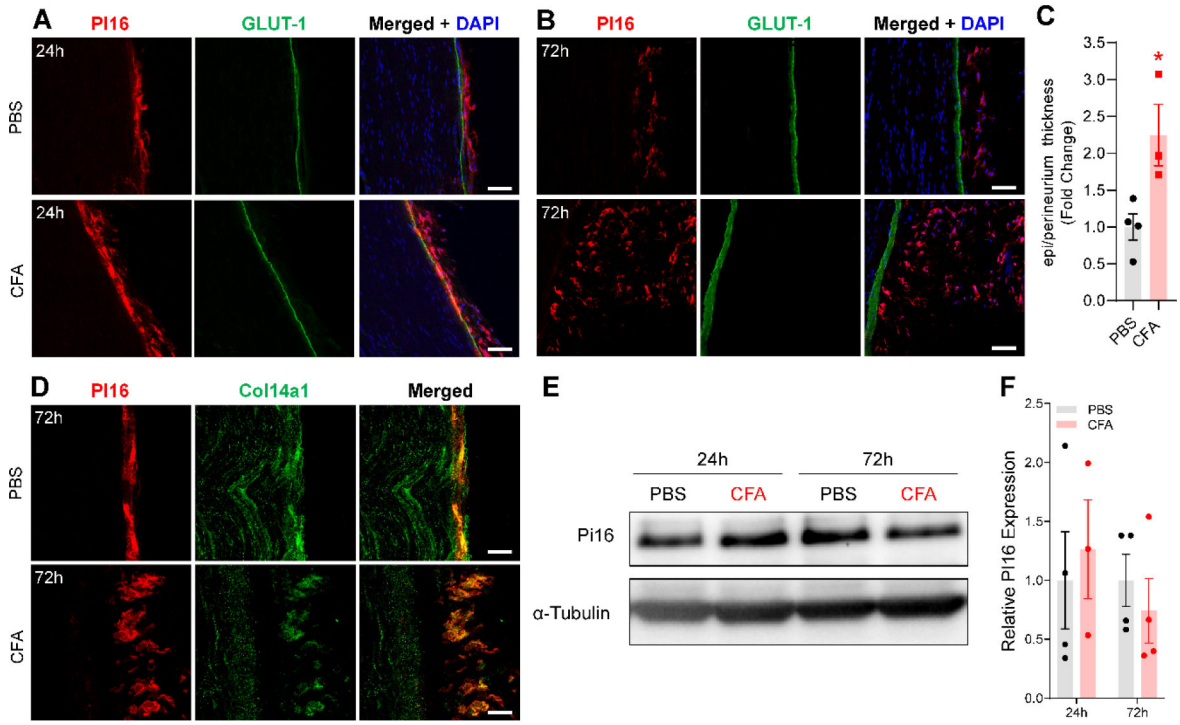

Fig. 3.

Effect of intraplantar CFA on PI16 protein expression. (A) Representative confocal image of sciatic nerve from PBS and CFA-treated female mice on day 1 of treatment showing immunostaining of PI16 (red) with outermost perineurial marker GLUT1 (green; B) from PBS and CFA-injected mice 3 days post-injection showing immunostaining of PI16 (red) with outermost perineurial marker GLUT1 (green). (C) Quantification of epineurium/perineurium thickness measured from perineurial marker GLUT1. Statistical analysis was performed using t-test: *P<0.05. (D) Representative image of PI16 (red) and Col14a1 (green) staining in the sciatic nerve on day 3 after CFA injection. Merged images show the co-localization of PI16 and Col14a1 (yellow), merged images in CFA show expansion of Col14a1 positive fibroblast in the epi/perineurium of the sciatic nerve co-expressing PI16. Immunofluorescence data are representative of n=4, each group (Scale bar 50 μm). (E) Representative Western blot and quantification of sciatic nerve PI16 24 or 72h after CFA injection in WT mice, quantified in (F).

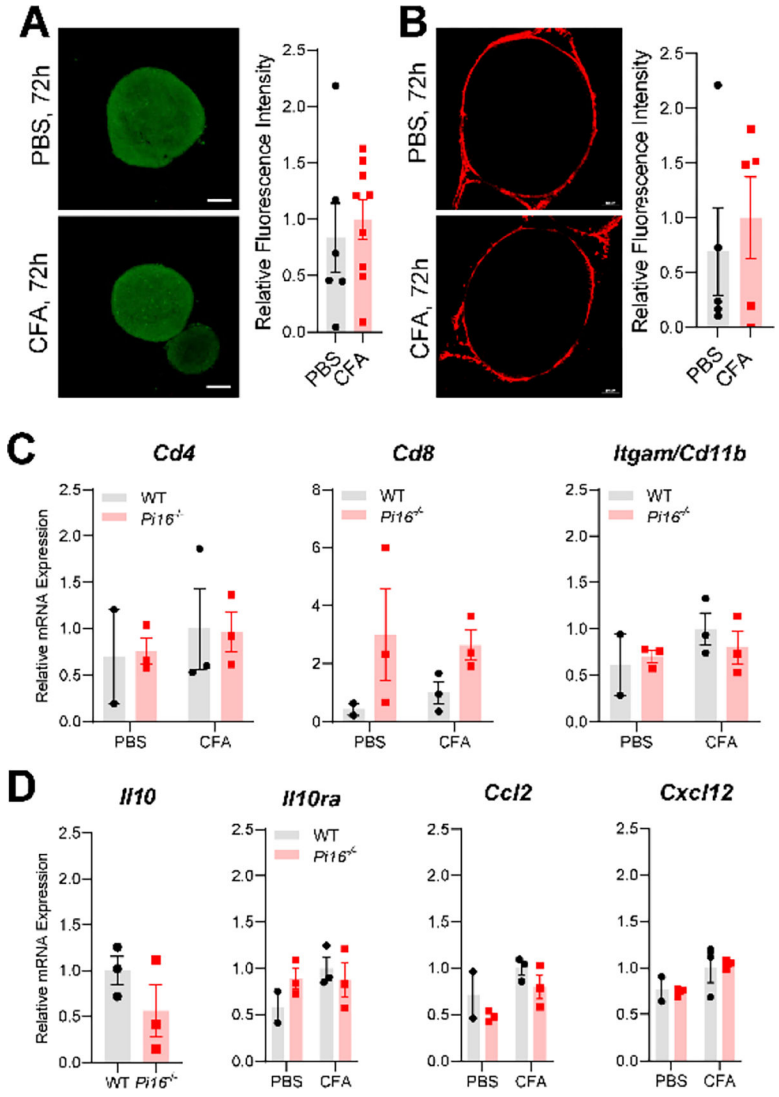

Fig. 4.

CFA does not affect sciatic nerve blood-nerve barrier permeability or inflammation. Representative image of sodium fluorescein (A) and Evans Blue Albumin (B) permeability in the sciatic nerves of female mice on day 3 following CFA or PBS controls (n=5, Scale bar 50 μm). (C) Quantification of leukocyte markers in the sciatic nerve on day 3 following CFA or PBS injection. (D) Quantification of cytokines/chemokines in the sciatic nerve on day 3 following CFA or PBS injection.

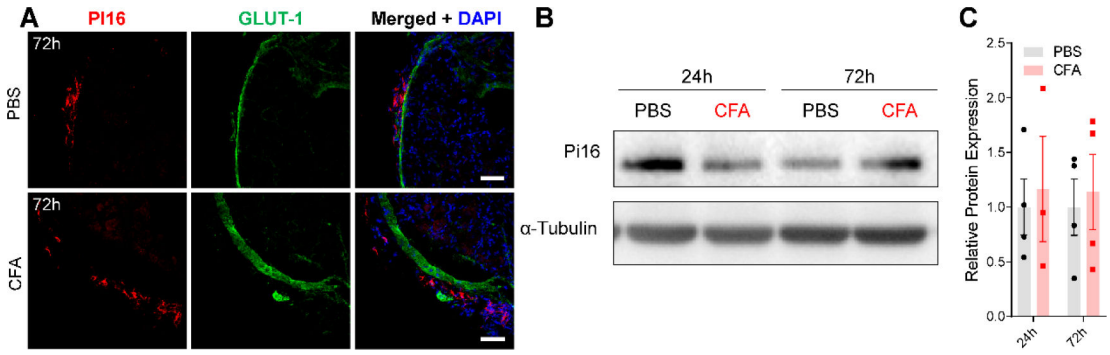

Fig. 5.

(A) Representative confocal image of DRG from PBS and CFA-injected female mice 3 days post-injection showing immunostaining of PI16 (red) with outermost perineurial marker GLUT1 (green). Immunofluorescence data are representative of n=4, each group (Scale bar: 50 μm). Representative Western blot (B) and quantification (C) of DRG PI16, 24 or 72h after CFA injection in WT female mice.

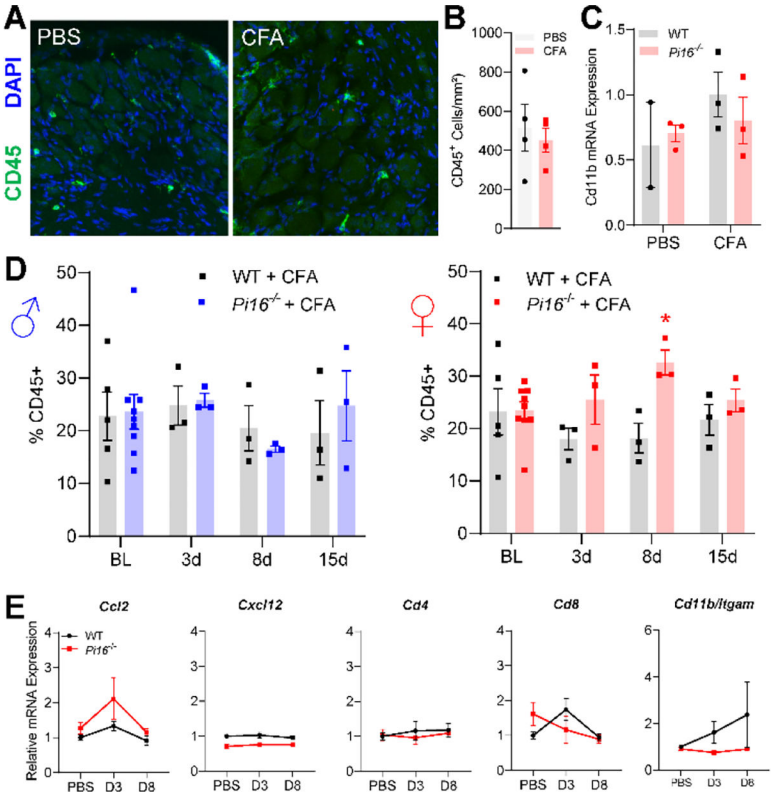

Fig. 6.

(A) Representative confocal images of DRG from PBS and CFA mice 3 days post-injection showing immunostaining of CD45 (green). DAPI (blue). Scale bar: 50 μm. CD45 density quantified in (B). (C) qPCR of *Cd11b* in WT and *Pi16*$^{-/-}$ DRG 3d after PBS or CFA injection shows no significant differences in transcript level. (D) Flow cytometry of lumbar DRG shows elevated CD45^{+} cell numbers selectively in female *Pi16*$^{-/-}$ at 8d post-CFA injection. (E) qPCR shows no significant differences between WT and *Pi16*$^{-/-}$ inflammatory marker expression in DRG after intraplantar CFA injection.

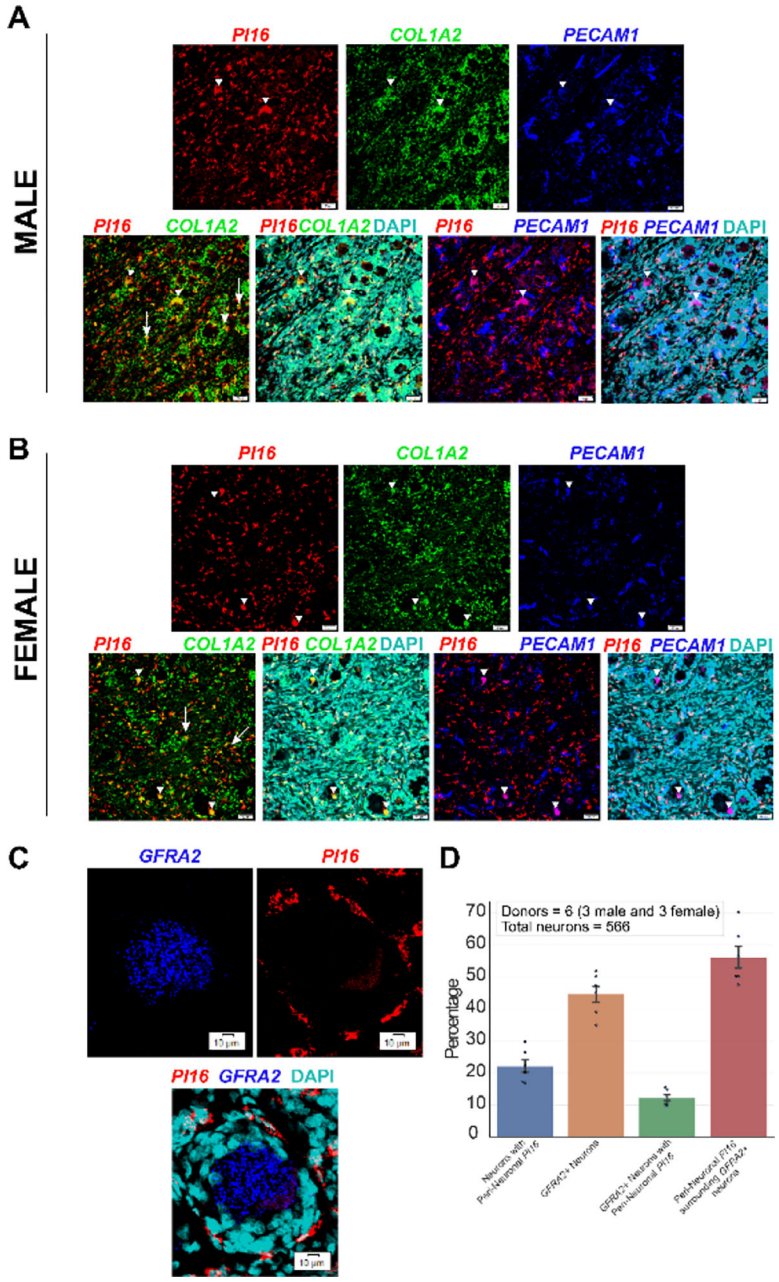

Fig. 7.

PI16 mRNA expression colocalizes with fibroblast marker *COL1A2* in human DRG and surrounds *GFRA2*+ neurons. *PI16* (red) expression overlaps with a subset of *COL1A2+* fibroblasts (green) but not with endothelial cell marker *PECAM1* (blue) in human DRGs recovered from male (A) and female (B) donors. Long arrows point to areas where *PI16* mRNA puncta overlap with *COL1A2* mRNA. White arrow heads show lipofuscin auto-fluorescence signal present in all channels. Scale bar = 50 μm. (C) *PI16* mRNA (red) surrounds neurons, including *GFRA2*+ neurons (blue) in human DRG. (D) Quantification of PI16 mRNA puncta shows that approximately 20% of all human DRG neurons have

peri-neuronal *PI16* and about 10% of *GFRA2*+ neurons have peri-neuronal PI16. Scale bar = 10 μm.

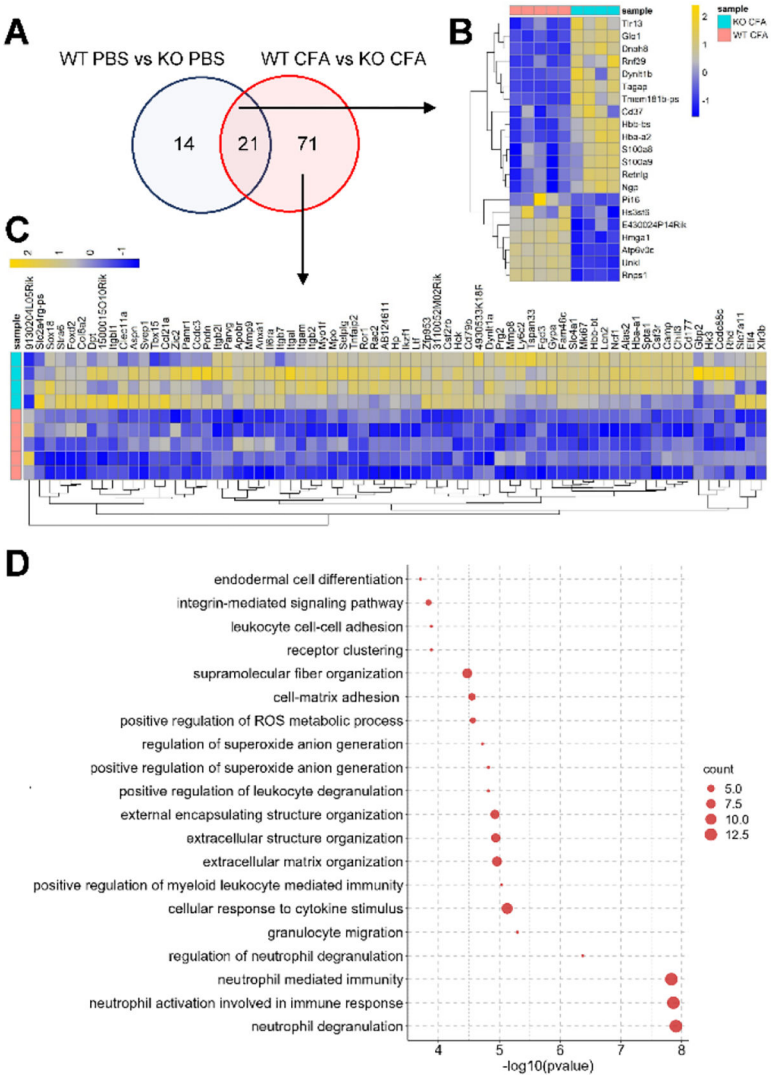

Fig. 8.

Bulk RNA sequencing of WT and *Pi16*$^{-/-}$ lumbar DRG shows increased myeloid cell signature 3d post-CFA injection. (A) Venn diagram illustrating the number of differentially-expressed genes in each dataset and their relative overlap. (B) Heat map depicting the 21 differentially-expressed genes common to PBS and CFA injection. (C) Heat map depicting the 71 differentially expressed genes in CFA-injected WT versus *Pi16*$^{-/-}$ mice. (D) Gene expression pathway enrichment analysis (WT CFA-injected versus *Pi16*$^{-/-}$ CFA-injected).

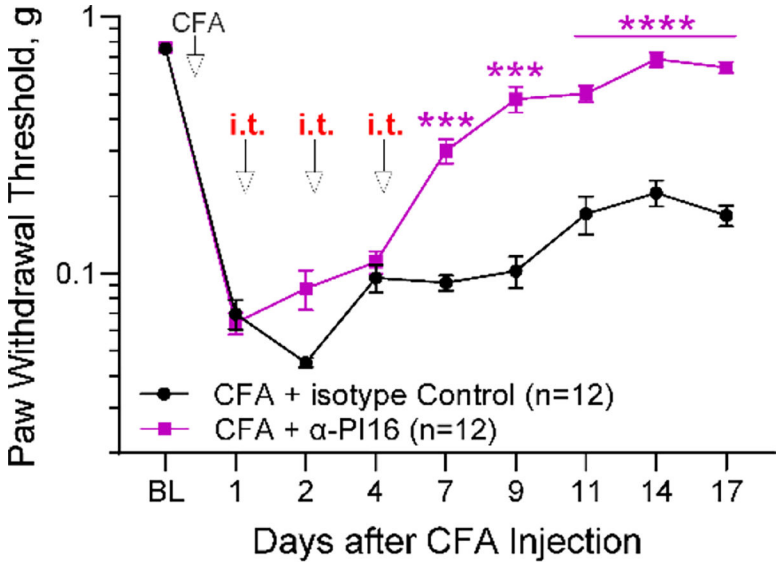

Fig. 9.

The effect of PI16 on inflammatory pain is mediated by extracellular PI16. anti-PI16 antibody or IgG isotype control were intrathecally injected (i.t.) on days 1, 2 and 4 following intraplantar CFA in WT female mice (n=12). On days where i.t. injections occurred, von Frey thresholds were measured prior to injections. Mice that received i.t. anti-PI16 show statistically significant recovery from CFA-induced hypersensitivity 7–17 days post-CFA. Two-way repeated-measures ANOVA, Bonferroni analysis: ***P<0.005, ****P<0.0001.

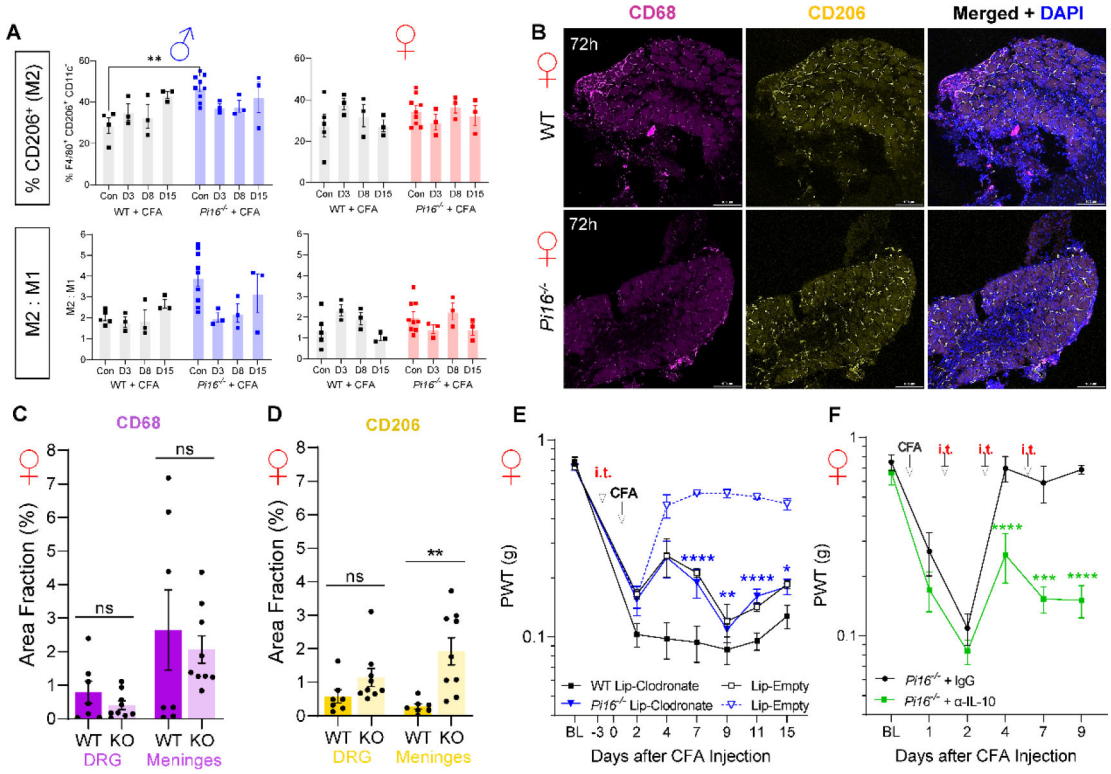

Fig. 10.

Role of CD206^{+} cells in resolution of CFA hypersensitivity in *Pi16*$^{-/-}$ mice. (A) Elevated F4/80^{+} CD206^{+} CD11c^{-} cells at baseline in male *Pi16*$^{-/-}$ DRG (left panels), with no significant differences observed in female DRG (right panels). (B) Representative IHC of CD206^{hi} labeling in female WT and *Pi16*$^{-/-}$ DRG, quantified in (C-D). A tendency toward decreased CD68 and increased CD206 density were observed in DRG parenchyma from *Pi16*$^{-/-}$ mice, with a statistically significant increase in meningeal CD206^{hi} cell density in *Pi16*$^{-/-}$. (E) Mrc1^{+} (CD206^{+}) Macrophages were depleted by intrathecal injection of mannosylated clodronate liposomes (Lip-Clodronate), 3 days prior to intraplantar injection of CFA. *Pi16*$^{-/-}$ mice that received Lip-Clodronate show prolonged hypersensitivity compared to *Pi16*$^{-/-}$ mice that received drug-free liposomes (Lip-Empty). Lip-Clodronate n=9, Lip-Empty n=3. (F) Following induction of inflammatory pain by intraplantar CFA injection in both hind paws, IL-10 was blocked by intrathecal injection of anti-IL-10 antibody or IgG isotype control on days 1, 2 and 4 post-CFA. On days of i.t. injection, von Frey thresholds were assessed prior to injections. *Pi16*$^{-/-}$ mice that received anti-IL-10 did not exhibit recovery from CFA-induced hypersensitivity (n=6). Two-way ANOVA, Bonferroni analysis: *P<0.05, **P<0.01, ***P<0.005, ****P<0.0001.

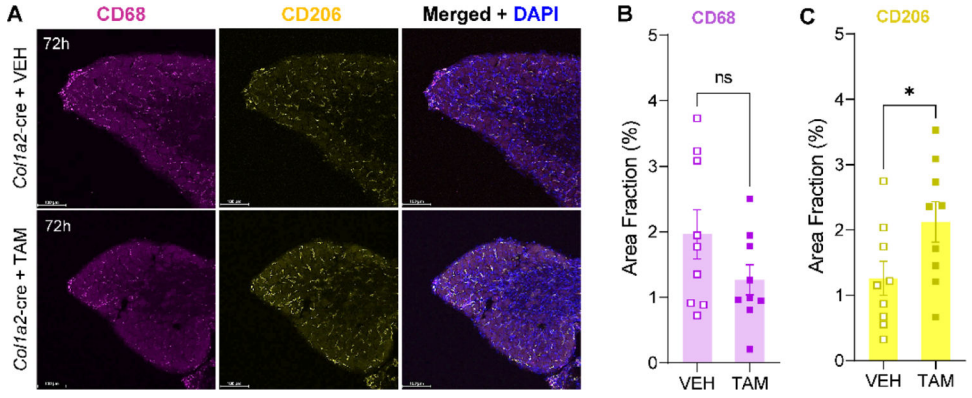

Fig. 11.

CD206^{hi} cells are elevated in DRG of fibroblast-specific *Pi16*$^{-/-}$ mice. (A) Representative IHC in vehicle (VEH) and tamoxifen-induced fibroblast *Pi16*$^{-/-}$ (*Col1a2*-cre) lumbar DRGs, 3 days after intraplantar CFA. (B) Total density of CD68^{+} cells in DRG shows a tendency toward reduction but is not significantly different in mice with fibroblast-specific deletion of PI16. (C) Significant increase in CD206^{hi} cell density in DRGs from mice with fibroblast-specific deletion of PI16. Student's T-test, *P<0.05.

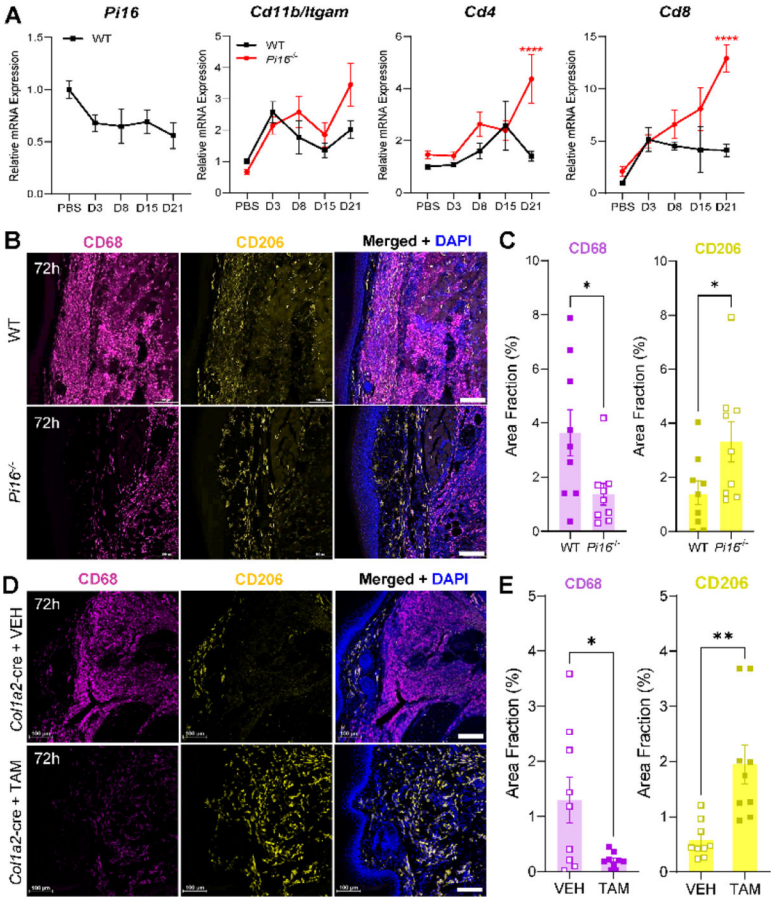

Fig. 12.

PI16 deletion is associated with reduced macrophage infiltration of hindpaw skin following CFA. (A) qPCR shows no significant expression changes in *Pi16* in WT skin, or *Itgam*/CD11b in female $Pi16^{-/-}$ versus WT hindpaw skin. Significant increases in expression of T-cell markers CD4 and CD8 occur only at late-stage timepoints. (B) Hindpaw skin shows significantly reduced CD68 (magenta) immunoreactivity along with an increase in the area fraction of $CD206^{hi}$ (yellow) cells in female $Pi16^{-/-}$ mice. DAPI: blue. Scale bar: 100 μm. (D) Representative IHC in vehicle (VEH) and tamoxifen-induced fibroblast PI16 knockout (*Col1a2*-cre) plantar hindpaw skin, 3 days after intraplantar CFA. (E) Significant decrease in $CD68^{+}$ cell density in skin from mice with fibroblast-specific deletion of PI16. Significant increase in $CD206^{hi}$ cell density in skin from mice with fibroblast-specific deletion of PI16. Student's T-test: *$P<0.05$, **$P<0.01$, Student's T-test.